JACS
JOURNAL OF THE AMERICAN CHEMICAL SOCIETY
Article
pubs.acs.org/JACS

Mollusk Shell Nacre Ultrastructure Correlates with Environmental Temperature and Pressure

Ian C. Olson,[†] Reinhard Kozdon,[‡] John W. Valley,[‡] and Pupa U. P. A. Gilbert*[,†,§]

[†]Department of Physics, University of Wisconsin—Madison, 1150 University Avenue, Madison, Wisconsin 53706, United States
[‡]WiscSims, Department of Geoscience, University of Wisconsin—Madison, 1215 West Dayton Street, Madison, Wisconsin 53706, United States
[§]Department of Chemistry, University of Wisconsin—Madison, 1101 University Avenue, Madison, Wisconsin 53706, United States

Supporting Information

ABSTRACT: Nacre, or mother-of-pearl, the tough, iridescent biomineral lining the inner side of some mollusk shells, has alternating biogenic aragonite (calcium carbonate, $CaCO_3$) tablet layers and organic sheets. Nacre has been common in the shells of mollusks since the Ordovician (450 million years ago) and is abundant and well-preserved in the fossil record, e.g., in ammonites. Therefore, if any measurable physical aspect of the nacre structure was correlated with environmental temperatures, one could obtain a structural paleothermometer of ancient climates. Using X-ray absorption near-edge structure (XANES) spectroscopy, Photoelectron emission spectromicroscopy (PEEM), and X-ray linear dichroism we acquired polarization-dependent imaging contrast (PIC) maps of pristine nacre in cross-section. The new PIC-map data reveal that the nacre ultrastructure (nacre tablet width, thickness, and angle spread) is species-specific in at least eight mollusk species from completely different environments: *Nautilus pompilius*, *Haliotis iris*, *Haliotis rufescens*, *Bathymodiolus azoricus*, *Atrina rigida*, *Lasmigona complanata*, *Pinctada margaritifera*, and *Mytilus californianus*. Nacre species-specificity is interpreted as a result of adaptation to diverging environments. We found strong correlation between nacre crystal misorientations and environmental temperature, further supported by secondary ion mass spectrometry measurements of *in situ* $\delta^{18}O$ in the nacre of one shell. This has far-reaching implications: nacre texture may be used as a paleothermometer of ancient climate, spanning 450 million years of Earth's history.

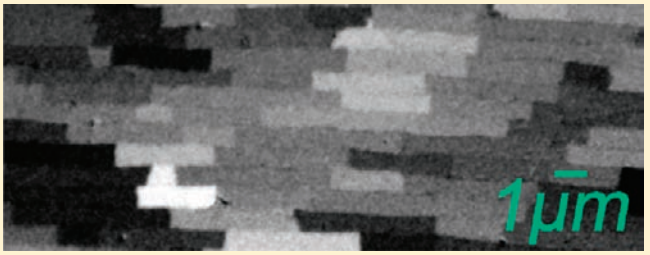

INTRODUCTION

The nacre organic−mineral composite comprises ∼2 wt % parallel organic sheets, alternating with aragonite crystals that constitute ∼98 wt % of the final material.[1,2] Nacre lining the inner surface of eight mollusk shells is shown in Figure 1. It has been widespread since the Ordovician, 450 million years ago.[3−5] Nacre is much more resilient than aragonite;[6−8] thus, its structure inspired the synthesis of novel materials.[9−11] Bivalves form sheet nacre,[12,13] while gastropods and cephalopods form columnar nacre.[1,14,15] Both kinds of nacre are formed by epithelial cells in the mollusk mantle and are made of irregular polygonal aragonite tablets, growing between predeposited, accurately spaced organic sheets. During their formation, however, sheet and columnar nacre differ significantly: on the growing surface of sheet nacre, only two or three consecutive layers of crystalline tablets are formed at once; while at the growing surface of columnar nacre, twenty or thirty layers of tablets are formed simultaneously and stacked into a column, with the bottom tablet larger and the overlying ones decreasing in size to form an approximately conical stack. Many columns are formed simultaneously; hence, the forming shell appears as conical pine trees in a forest (see Figure 2). Despite these different formation geometries, the resulting nacre appears similar in visual appearance across species, as shown in Figure 1.

We analyzed nacre from eight species of mollusks that live in dramatically different environments: in fresh and salt water, ranging in depth from 1 to 2300 m and temperature from 0°C to 32°C. During the course of nacre evolution, or during the life of a single organism, nacre structural parameters may have changed, in adaptation to changing environmental conditions and locations. In order to detect the existence of such effects, we selected a diverse set of eight modern mollusk species: five bivalves, one cephalopod, and two gastropods, all shown in Figure 1.

Metzler et al. reported the first observation of X-ray linear dichroism[21,22] in X-ray absorption near-edge structure (XANES) spectroscopy of calcite and aragonite and observed this effect in mollusk shell nacre from red abalone (*Haliotis rufescens*).[14,18,23] They used this effect to display contrast between nacre tablets by photoelectron emission spectromicroscopy (PEEM) but with a non-quantitative approach to polarization-dependent imaging contrast (PIC) mapping. A

Received: November 16, 2011
Published: February 7, 2012

   dx.doi.org/10.1021/ja210808s | J. Am. Chem. Soc. 2012, 134, 7351−7358

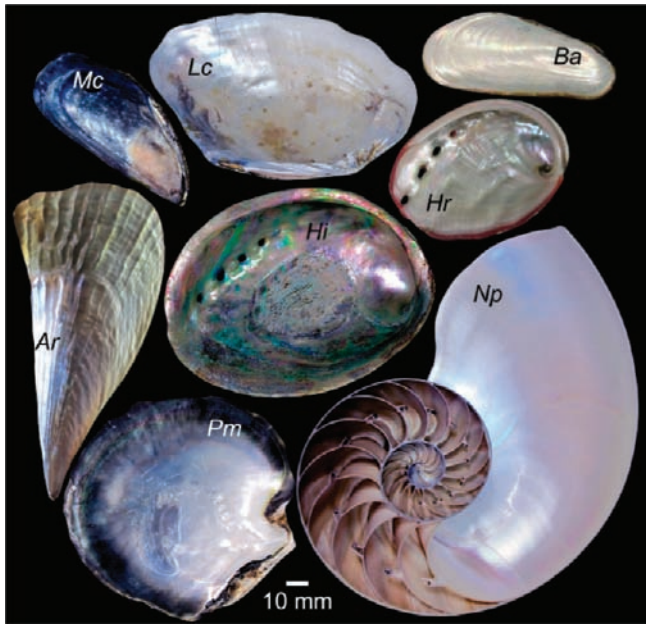

Figure 1. Photographs of the eight mollusk shells studied here: *Np*: *Nautilus pompilius*, the emperor nautilus collected off the coast of Jolo Island, Philippines. *Hi*: *Haliotis iris*, the paua shell, or blackfoot abalone from New Zealand. *Hr*: *Haliotis rufescens*, the red abalone from Santa Cruz, CA. *Ba*: *Bathymodiolus azoricus*, a deep-sea mussel from the Mid-Atlantic Ridge collected by a robot 850 m under the water surface. *Ar*: *Atrina rigida*, the pen shell from Sanibel Island, FL. *Lc*: *Lasmigona complanata*, a freshwater mussel from the shallow waters of the Milwaukee River, WI. *Pm*: *Pinctada margaritifera*, the Tahitian black pearl oyster from Rangiroa Island, French Polynesia. *Mc*: *Mytilus californianus*, the oceanic black mussel from the intertidal zone in Bolinas, CA. All images have the same scale bar.

method to quantitatively measure the orientation of tablets in nacre, although most desirable, remained elusive until recently, as described for calcite nanocrystals.[24] In this study, we present the first experimental results of quantitative orientation measurements for each aragonite crystal, with respect to the linear polarization vector.

The method used here is also termed PIC-mapping and uses XANES-PEEM. This version of PIC-mapping provides simultaneous measurement of three ultrastructural parameters: thickness, width, and crystal orientation for each aragonite tablet, in large cross-sectioned arrays of nacre tablets in their pristine mutual arrangement. In one sample, XANES-PEEM maps were combined with *in situ* measurements of $\delta^{18}O$ by ion microprobe in immediately adjacent regions.

RESULTS

Figure 3 shows PIC-maps of nacre from each of the eight species. In these PIC-maps the gray level represents the orientation of the aragonite crystal *c*-axis. The *c*-axis is defined here as follows: at the atomic scale, each CO_3 group in the aragonite structure forms a plane, and all CO_3 planes are parallel to one another and perpendicular to the *c*-axis.

The linear polarization vector (magenta arrow in Figure 3) can be rotated in the plane perpendicular to the X-ray direction, shaded in magenta. For each image acquired, the orientation of this vector is defined by the elliptically polarizing undulator (EPU) angle, labeled EPU°. The angle between the *c*-axis and this vector is called θ, which we cannot directly measure. What we can and do measure quantitatively is the θ' angle between

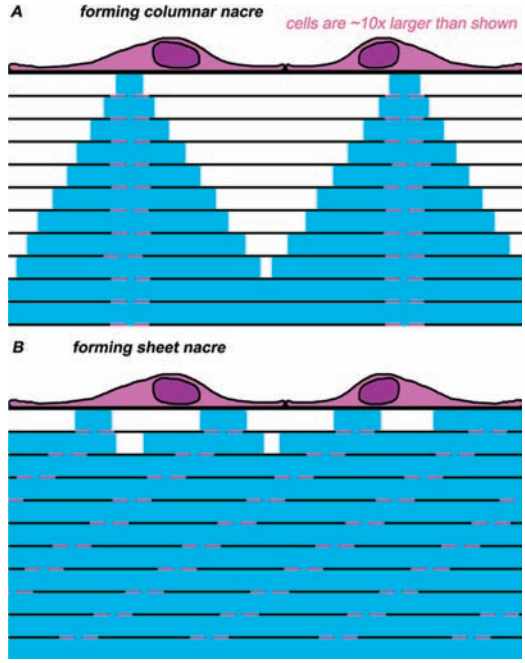

Figure 2. Schematic representations of forming nacre. (A) Columnar nacre formed by gastropods and cephalopods. (B) Sheet nacre formed by bivalves. These schematics are adapted from Addadi and Weiner,[1] combined with Nudelman et al.,[16] Schäffer et al.,[17] Gilbert et al.[18] and observations in this work. In both schematics the organic sheets are represented by horizontal black lines; the nucleation sites, which are also organic,[16] are magenta donuts with a hole at their center; aragonite tablets are light blue, and mantle cells at the top are magenta. The nacre growth direction perpendicular to the organic sheets is oriented from bottom to top. (A) The bottom two layers of aragonite tablets are fully formed and have filled all available space. Those in the third layer are still growing and will soon close the white gap at the center and stop growing when they abut one another. The fourth layer tablets will then follow and so on up to the 11th layer displayed (see for example ref 19). (B) Nine sheet-nacre aragonite layers have filled space, while only two are currently forming (see, for example, images of forming nacre from *Atrina rigida* in Nudelman et al.[16]). Notice that the organic nucleation sites are stacked approximately on top of one another in columnar nacre but staggered diagonally in sheet nacre. This arrangement is deduced from the PIC maps of nacre cross-sections in this work. In Figure 3 the columnar nacre in *Np*, *Hi*, and *Hr* clearly shows stacks of co-oriented single-crystalline tablets, with their stacking axis approximately perpendicular to the nacre layers. Sheet nacre, instead, often has staggered stacks of co-oriented tablets, as is most evident in *Pm* and *Mc* PIC-maps in Figure 3. Co-orientation in these stacks is maintained by mineral bridges traversing the organic sheets, as first described by Schäffer et al.[17] Notice that there cannot be multiple mineral bridges per tablet. If there were multiple pores through the organic sheets, and therefore multiple nucleation sites per tablet, then, in one nacre layer, nacre tablets would have jagged edges and not smooth, straight, or slightly curved polygonal edges.[18] The polygonal shape of nacre tablets, invariably observed in columnar and sheet nacre, can only result from one nucleation site per tablet, as in a Voronoi construction.[18,20] This geometrical prediction was verified experimentally by Nudelman et al.,[16] who indeed found one nucleation site per tablet, which contains nucleating proteins highly conserved across species. This nucleation site is organic; thus, it must not be continuous but porous, so the underlying crystal can bridge through it and propagate its orientation to the nucleating tablet above. This is why we represent the nucleation sites as magenta donuts in cross-section, with a pore at their center. Each tablet starts its growth from these sites, though these are not rigorously nucleation sites as no new nucleation event occurs for each tablet.

dx.doi.org/10.1021/ja210808s | J. Am. Chem. Soc. 2012, 134, 7351−7358

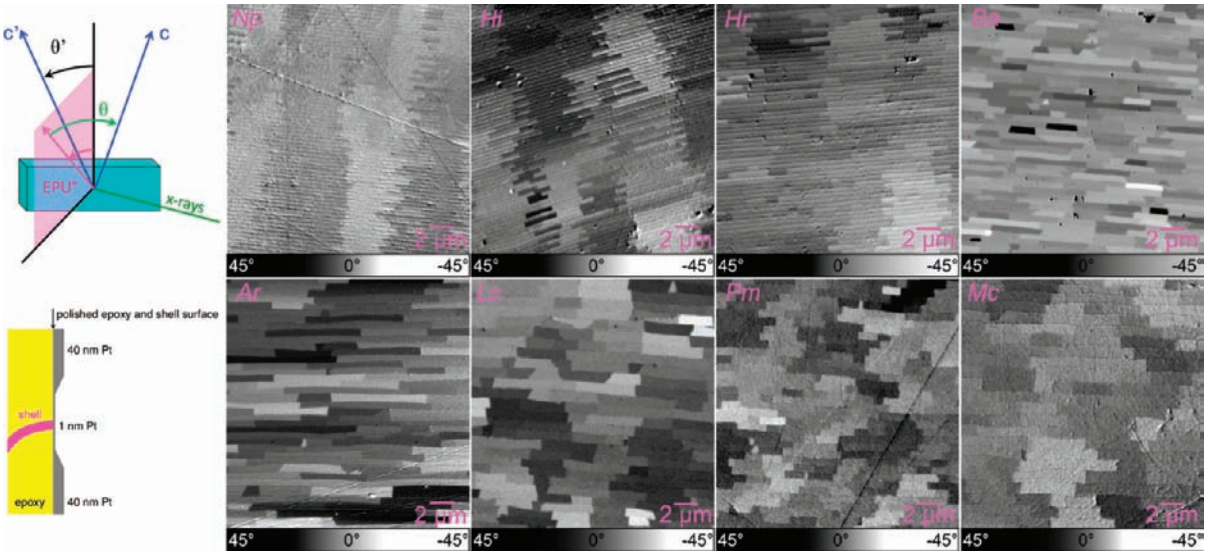

Figure 3. PIC-maps of nacre from the eight shells, labeled as in Figure 1. The samples are all normal cross-sections; thus, the nacre layer planes are perpendicular to the plane of the image and the nacre growth direction is from bottom to top. The schematic on the top-left shows one nacre tablet (cyan cuboid), the direction of the illuminating X-ray beam, and the magenta plane in which the EPU angle can be rotated. The schematic on the bottom-left shows how the shells (magenta) were embedded into epoxy (yellow), polished, and then coated with platinum (gray).[25,26] The PIC-maps in grayscale show the angle θ' between the vertical direction, which, because the sample is mounted vertically, is always in-plane on the sample surface, and the projection of the aragonite crystal *c*-axis onto the magenta plane, as shown in the schematic on top-left. In PIC-maps *Np*, *Hi*, *Hr*, *Ba*, *Ar*, *Lc*, *Pm*, and *Mc* the gray level quantitatively represents the orientation of the *c*′-axis, according to the grayscale bar at the bottom of each PIC-map. Notice in each map the differences in orientation of tablets, and in tablet width and thickness. Data from these and many other PIC-maps are summarized in Table 1.

the vertical direction and the *c*′-axis, that is, the projection of the *c*-axis onto the magenta plane.[24] In Figure 3, the PIC-maps display in gray levels the crystal orientation of each nacre tablet, with different θ' angles corresponding to different gray levels according to the grayscale bars under each map.

Several observations stand out in Figure 3. First, each tablet behaves as a single crystal of aragonite, as expected.[19,27−30] Second, immediately adjacent tablets in the same nacre layer do not have the same orientation; we observe tablets in the same nacre layer with *c*′-axes spread by as much as 45° in *Ba*, 32° in *Lc*, 28° in *Pm*, 19° in *Ar*, 18° in *Mc*, 18° in *Hi*, 16° in *Hr*, and 6° in *Np*. This quantitative observation of large angle spread is unprecedented and counterintuitive. The tablet-to-tablet boundaries are flat, but these are not crystal faces and have no correlation with crystal orientations. Most other authors have stated that the *c*-axis in mollusk shell nacre is oriented perpendicular to the shell surface and has the same orientation for all tablets in nacre.[31−35] This statement is inaccurate at the microscopic scale. The spread in orientation is species-specific and can be visually appreciated at a glance in Figure 3: co-oriented tablets would appear homogeneously gray in PIC-maps while Figure 3 shows great tablet contrast. Third, the tablet widths and thicknesses are very different across the different species and again are species-specific, as shown in Table 1. The tablet widths are clearly visible and measurable in PIC-maps such as those in Figure 3, as the different crystal orientations highlight the exact location where one tablet ends and the adjacent tablet begins in each nacre layer. Fourth, we observe that the columnar nacre formed by the cephalopod *Np* exhibits very tall, straight stacks of tablets that share the same orientation (gray level), while adjacent columns have different orientations. Co-orientation in each stack of tablets must be transmitted via mineral bridges as described previously[17,18,36,37] and in Figure 2. In gastropod columnar nacre from *Hi* and *Hr* the columns are also straight, in agreement with previous observations in *Haliotis rufescens*.[18,38] In the sheet nacre formed by the five bivalves, instead, stacks of co-oriented tablets include very few (one to six) tablets as seen in these cross-sections, are never straight, and in *Mc* and *Pm* are staggered. These observations of differences in nacre architecture between the bivalve and gastropod−cephalopod nacre are consistent with those observed by Wise,[19,27] Erben,[39] and Mutvei.[3,4,40−42] The aragonite twinning within each tablet shown by Mutvei[40] is not detectable with PIC-mapping, because PIC-mapping is only sensitive to *c*-axis orientations and not to rotations around the *c*-axis as occur in aragonite twinning.[18]

The width of a tablet in a nacre cross-section strongly depends on where the cross-section is taken. A polygonal tablet polished near a vertex of the polygon would appear smaller; one polished near its center would appear larger. Hence, the absolute width measured on one tablet does not represent a meaningful parameter. The average of all tablet widths in a PIC-map, however, is a meaningful parameter and has a value characteristic of each mollusk species. Correspondingly, the error bars on the average tablet width are large, as reported in Table 1. Average tablet widths are between 3 and 4 μm in most bivalves but much larger, up to 8 μm, in *Ar*.

All three ultrastructural parameters, angle spread, tablet width, and tablet thickness, are species-specific. We interpret the specificity as a result of adaptation to changing environments. As the environmental changes occurred, each genus and species may have adapted by regulating nacre ultrastructural parameters.

In order to test for correlations between the structural and the environmental parameters reported in Table 1, we plotted each parameter as a function of all others and observed their correlation coefficients, as reported in Table 2. Thus, instead of formulating *a priori* hypotheses on which factors influenced

dx.doi.org/10.1021/ja210808s | J. Am. Chem. Soc. 2012, 134, 7351−7358

Table 1. Measurements of Average Tablet Widths, Thicknesses, and Angle Spread of Tablet Crystal *c*′-Axis Orientations from Individual PIC-Maps[a]

species name	PIC-map	distance from NP boundary (μm)	tablet width ± StDev (μm)	no. of tablet widths averaged	tablet thickness ± StDev (μm)	no. of tablet thicknesses averaged	angle spread footprint (degrees)	tablets in image	max pressure (bar)	95th %ile temperature (°C)	5th %ile temperature (°C)	mean annual temperature (°C)
Atrina rigida	Ar-12	180	6.38 ± 3.72	58	0.64 ± 0.03	136	43	134	3.7[43]	31.9[44]	18.5[44]	25.9[44]
Atrina rigida	Ar-13	200	7.44 ± 4.32	42	0.67 ± 0.03	150	43	110	3.7[43]	31.9[44]	18.5[44]	25.9[44]
Atrina rigida	Ar-14	220	8.04 ± 3.76	31	0.69 ± 0.03	151	42	101	3.7[43]	31.9[44]	18.5[44]	25.9[44]
Bathymodiolus azoricus	Ba-6	251	3.28 ± 1.59	50	0.46 ± 0.09	55	35	439	230[45]	–	–	–
Bathymodiolus azoricus	Ba-7	251	3.28 ± 1.59	50	0.46 ± 0.09	55	45	439	230[45]	–	–	–
Bathymodiolus azoricus	Ba-8	191	3.65 ± 1.54	50	0.62 ± 0.09	40	81	285	230[45]	–	–	–
Bathymodiolus azoricus	Ba-9	191	3.65 ± 1.54	50	0.62 ± 0.09	40	77	285	230[45]	–	–	–
Bathymodiolus azoricus	Ba-17	100	3.14 ± 1.48	31	0.59 ± 0.09	71	101	213	230[45]	–	–	–
Haliotis iris	Hi-57	200	2.81 ± 1.86	54	0.37 ± 0.01	291	54	350	2.52[46]	20[47]	8[47]	14[47]
Haliotis iris	Hi-58	220	4.02 ± 1.85	77	0.39 ± 0.01	213	46	285	2.52[46]	20[47]	8[47]	14[47]
Haliotis iris	Hi-59	240	2.42 ± 1.82	52	0.38 ± 0.01	242	48	361	2.52[46]	20[47]	8[47]	14[47]
Haliotis rufescens	Hr-27	191	3.96 ± 2.23	28	0.46 ± 0.02	112	62	201	19.1[48]	16.1[49]	11.6[49]	13.6[49]
Haliotis rufescens	Hr-28	208	4.25 ± 1.44	27	0.43 ± 0.02	149	51	207	19.1[48]	16.1[49]	11.6[49]	13.6[49]
Haliotis rufescens	Hr-45	212	4.98 ± 2.02	53	0.45 ± 0.02	185	65	221	19.1[48]	16.1[49]	11.6[49]	13.6[49]
Haliotis rufescens	Hr-46	232	3.69 ± 1.73	51	0.43 ± 0.02	201	55	219	19.1[48]	16.1[49]	11.6[49]	13.6[49]
Lasmigona complanata	Lc-10	140	3.48 ± 1.83	50	0.67 ± 0.21	63	41	229	1.1[50]	25[51]	0[51]	12[51]
Lasmigona complanata	Lc-11	170	3.59 ± 1.93	26	0.85 ± 0.21	49	42	153	1.1[50]	25[51]	0[51]	12[51]
Lasmigona complanata	Lc-12	200	3.53 ± 2.12	50	1.10 ± 0.21	38	34	126	1.1[50]	25[51]	0[51]	12[51]
Mytilus californianus	Mc-10	40	4.05 ± 2.20	31	0.87 ± 0.02	31	35	124	4.0[52]	15.2[53]	9.7[53]	12.1[53]
Mytilus californianus	Mc-15	220	4.10 ± 1.80	17	0.88 ± 0.02	17	35	108	4.0[52]	15.2[53]	9.7[53]	12.1[53]
Mytilus californianus	Mc-16	320	4.20 ± 2.10	41	0.84 ± 0.02	41	36	115	4.0[52]	15.2[53]	9.7[53]	12.1[53]
Nautilus pompilius	Np-9	100	3.83 ± 1.85	74	0.32 ± 0.02	172	51	372	51.3[54]	20[55,56]	7.1[55,56]	18[55,56]
Nautilus pompilius	Np-26	220	5.54 ± 2.93	24	0.33 ± 0.02	24	38	240	51.3[54]	20[55,56]	7.1[55,56]	18[55,56]
Nautilus pompilius	Np-27	320	6.52 ± 2.13	14	0.28 ± 0.02	14	30	309	51.3[54]	20[55,56]	7.1[55,56]	18[55,56]
Nautilus pompilius	Np2-11	170	2.75 ± 0.94	50	0.30 ± 0.02	150	46	484	51.3[54]	20[55,56]	7.1[55,56]	18[55,56]
Nautilus pompilius	Np2-12	187	3.04 ± 1.01	44	0.28 ± 0.02	150	45	525	51.3[54]	20[55,56]	7.1[55,56]	18[55,56]
Nautilus pompilius	Np2-13	204	2.71 ± 1.04	50	0.31 ± 0.02	156	43	524	51.3[54]	20[55,56]	7.1[55,56]	18[55,56]
Pinctada margaritifera	*Pm*-8	120	3.48 ± 2.36	50	0.68 ± 0.01	68	31	256	5.1[57]	29.8[58]	27.6[58]	28.7[58]
Pinctada margaritifera	*Pm*-34	53	3.59 ± 1.31	26	0.66 ± 0.01	26	38	242	5.1[57]	29.8[58]	27.6[58]	28.7[58]
Pinctada margaritifera	*Pm*-40	140	3.27 ± 1.70	76	0.67 ± 0.01	70	44	212	5.1[57]	29.8[58]	27.6[58]	28.7[58]

[a]We also report the distance from the nacre-prismatic (NP) boundary for each analyzed area, and hydrostatic pressure and temperature data for each specimen. Each tablet width measurement was averaged over 14−77 data points. The tablet thicknesses were averaged over 14−291 data points. The standard deviations are indicated next to tablet widths and thicknesses. For tablet widths, the standard deviation is large, for the reasons explained in the text. The angle-spread measurements were performed over 101−525 tablets. Environmental temperatures were determined based on extensive temperature data sets, from which the 95th percentile temperature measurement was selected to represent the maximum and the 5th percentile the minimum temperature at the locations where the shells were collected. For *Ba*, we only know the temperature measured at the time of collection, which was 8.5°C,[45] and we do not have extensive data as a function of time; hence, we can't report the maximum, minimum, and mean annual temperatures.

dx.doi.org/10.1021/ja210808s | J. Am. Chem. Soc. 2012, 134, 7351−7358

Table 2. Correlation of Structural Parameters (tablet thickness, width, angle spread) and Environmental Parameters (maximum hydrostatic pressure, minimum, maximum, and mean annual temperature)[a]

correlation coefficient	Tablet Width	Tablet Thickness	Angle Spread	Max Pressure	Max Temperature	Min Temperature	Mean Annual Temperature
R=1.00-0.70							
R=0.70-0.40							
R=0.40-0.00							
Tablet Width		13%	8%	6%	42%	18%	34%
Tablet Thickness	13%		55%	76%	28%	1%	9%
Angle Spread	8%	55%		10%	82%	13%	48%
Max Pressure	6%	76%	10%		33%	13%	5%
Max Temperature	42%	28%	82%	33%		52%	79%
Min Temperature	18%	1%	13%	13%	52%		86%
Mean Annual Temperature	34%	9%	48%	5%	79%	86%	

[a]The correlation coefficient R varies between 0 and 1, for parameters correlated 0% and 100%, respectively. We color-coded the R-values for each pair of parameters in this table, according to the legend on top left. White cells indicate uninteresting parameter correlations. The tablet width and angle spread measurements are further described in Methods Summary. The angle spread is strongly correlated with the maximum temperature (82%), while the tablet thickness is strongly correlated with maximum pressure (76%) (see Figures 4 and 5); hence, we will only consider these most striking results and neglect the weaker correlations at this time.

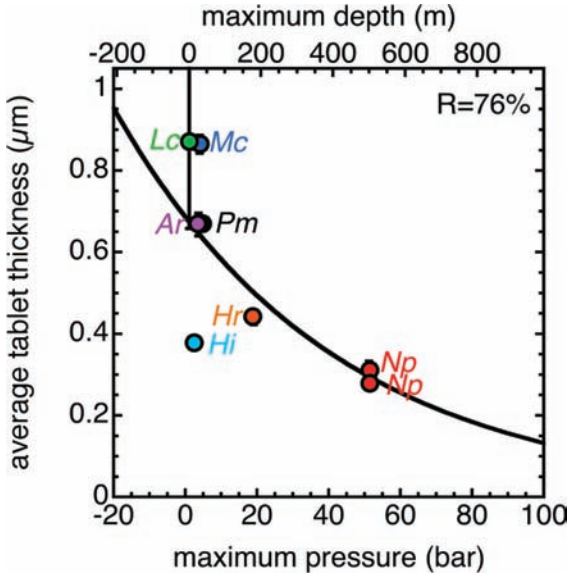

Figure 4. The average nacre tablet thickness decreases as the maximum depth or maximum hydrostatic pressure increases. The latter are the maximum pressures experienced by each nacre-forming mollusk species, labeled as in Figures 1 and 3. Tablet thickness data were averaged for each species. The vertical error bars represent the standard deviation of the three to six average thicknesses per species shown in Table 1, and for several data points they are smaller than the marker. The *Np* data were acquired from two different shells from different locations and show excellent reproducibility. The black curve is an exponential fit of the data, with correlation coefficient R = 76%. Clearly the *Hi* shell, with its very small tablet thickness, is an outlier, but this data-point is included in the exponential fit and the correlation is still strong (excluding this data-point makes the fit far better, with R = 94%).

nacre ultrastructure during the course of its evolution,[59] or during the life of a single organism, we measured all parameters and let them suggest any possible effects by showing strong correlations. This approach represents a first step toward more refined hypotheses, which will then be tested on a more focused set of mollusk shell samples.

The only two pairs of parameters that are strongly correlated in Table 2 are the angle spread with maximum temperature, and tablet thickness with maximum pressure. Interestingly, the minimum temperatures do not appear to play any role (R = 13%) in nacre structure, while the maximum temperatures do (R = 82%). The mean annual temperature shows an intermediate correlation coefficient (R = 48%), which can be assumed to depend only on the maximum temperatures. Hence, the minimum and mean temperature can be neglected in an analysis of nacre structural parameters. We now present a more in-depth analysis of the strongly correlated parameters observed from Table 2, discuss their significance, and formulate two new hypotheses.

Tablet thicknesses vary dramatically in Table 1, by a factor of 4, from 0.28 to 1.10 μm for *Np* and *Lc*, respectively. Assuming that the thickness of the organic sheets separating nacre tablet layers is uniform across all species, thinner tablets in some species result in significantly larger ratios of organic/crystalline nacre components compared with thick-tablet nacre. This may be the result of slower metabolic rate at higher pressures. Alternatively, if this organic material serves to resist fracture by absorbing energy[60] or enabling tablet sliding and locking,[61] this observation may indicate that nacre from the deep-sea shells *Hr*, *Np*, and *Ba* is likely more resistant to fracture than nacre from other species, consistent with Currey's observation that nacre with thicker layers is weaker[6] and Mutvei's observation that a much larger fraction of organic components rendered ancient nacre far more flexible than modern nacre.[3,59] The plot in Figure 4 demonstrates the trend of decreasing tablet thickness with increasing maximum hydrostatic pressure. Future mechanical tests on nacre tensile and compressive strength, as well as fracture toughness, might substantiate the hypothesis presented here that nacre tablet thickness is inversely proportional to mechanical resilience. For now, we just remark upon the strong correlation (76%) of tablet thickness with depth.

For each PIC-map of each area, we extracted the histogram of c'-axis angles, as shown in Table 1 and Supporting Information Figures S1–S4. We then measured the footprint of each histogram and termed it "angle spread". All angle spreads are reported in Table 1 and are in reasonable agreement with previous X-ray diffraction data obtained for red abalone (*Hi* and *Hr* give 34° and 35° here) by measuring the footprint of a rocking curve (22°)[23] or the footprint of a pole figure (32°).[36,62] We then averaged all angle spreads measured for each species and plotted them as a function of minimum, maximum, and mean annual temperature. Only one of these plots produces a strikingly high 82% correlation: the plot with maximum environmental temperature, as presented in Figure 5.

In both Figures 4 and 5 we omitted data for *Ba*, a mussel collected in deep water on the Mid-Atlantic ridge. Maximum

dx.doi.org/10.1021/ja210808s | J. Am. Chem. Soc. 2012, 134, 7351–7358

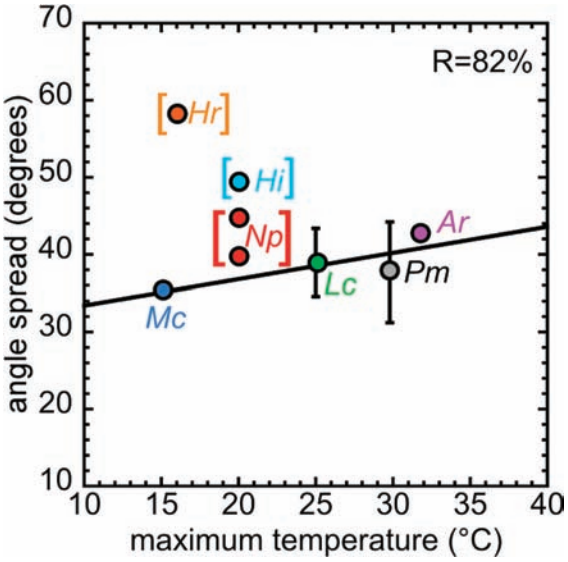

Figure 5. A strong correlation is observed between maximum environmental temperature and the average angle spread in each nacre-forming mollusk species, labeled as in Figures 1, 3, and 4. Angle spread data were averaged for each species. The vertical error bars represent the standard deviation of the averaged angle spreads, while the horizontal error bars are ±0.1°C, estimated by comparing the 95% ile maximum temperatures for subsequent years in each location. (Only the bivalve data were included in this linear fit, represented by the black line. The *Hr*, *Hi*, and *Np* data-points are excluded from the fit. Including these points makes the fit far worse, with R = 33%). Again *Np* shows excellent reproducibility.

temperature data are not available for *Ba.* In both Figures 4 and 5, *Ba* is an outlier, with an averaged angle spread of (67.8 ± 27.2)°, an average tablet thickness of (0.55 ± 0.09) μm, and a maximum pressure of 230 bar. This deep-sea shell, thriving around hydrothermal vents, may have followed its own path in evolution, generating the discrepancy in nacre structure observed here.

In Figure 6 we present angle spread data and oxygen stable isotope data, acquired *in situ* by secondary ion mass spectrometry (SIMS) with 10 μm beam spot size from the same nacre regions in one *Pm* shell. $\delta^{18}O$ data are sensitive to the environmental temperature at the time of calcium carbonate deposition.[63−65] If the oxygen isotope ratio ($^{18}O/^{16}O$, expressed as $\delta^{18}O$) of seawater was constant during the lifetime of the *Pm* mollusk, then $\delta^{18}O$ will be lower (more negative) at higher water temperatures.[63−65] Thus the correlation of minima in $\delta^{18}O$ and maxima in angle spread data (green dots, Figure 6) strongly supports the hypothesis that nacre angle spread corresponds to variations in environmental temperature, as suggested by the results of Figure 5.

■ DISCUSSION

Previous studies addressed the effect of water temperature on mollusk shell aragonite/calcite ratio,[66,67] on oxygen and carbon isotopic fractionation,[68] and on nacre tablet morphology.[69] Other studies looked at the effect of Mg/Ca ratio in seawater on the mollusk shell aragonite/calcite ratio,[70] and the effect of pressure on nacre ultrastructure.[45] All these studies measured variations in water composition, temperature, or pressure over time. The present study differs, in that it does not formulate *a priori* hypotheses but uses an *a posteriori* approach: we measured structural and environmental parameters, plotted

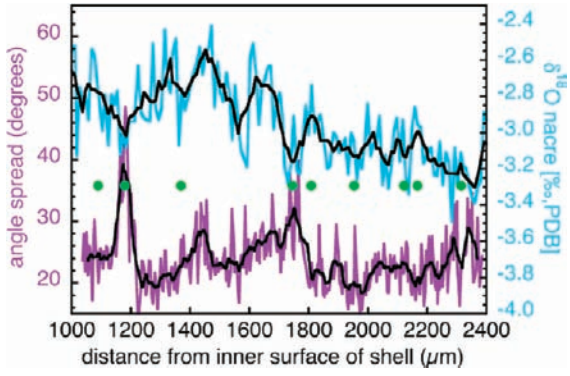

Figure 6. Angle spread data and $\delta^{18}O$ data derived from the ratio of $^{18}O/^{16}O$ concentrations, obtained by secondary ion mass spectrometry (SIMS) from 140 spots, each 10 μm in diameter, 1 μm deep, and 10 μm apart, collected from a *Pm* shell cross-section. The SIMS pits were identified in PEEM, and angle spread data were acquired from immediately adjacent regions, which were formed nearly simultaneously by the mollusk. The angle spread data were extracted from 68 PIC-maps, spanning a distance of 1400 μm. Both plot lines for $\delta^{18}O$ and angle spread were smoothed (black line), over five and nine data points respectively, to facilitate comparison of the two plots. $\delta^{18}O$ is lower (more negative) at higher temperature; therefore, dips in $\delta^{18}O$ are expected to align with peaks in angle spread. Although the data are noisy and the alignment of maxima and minima is not perfect, in several regions the alignment is acceptable. The positions in nacre in which maxima and minima align are highlighted by green dots in the figure.

them in pairs, and let an unbiased correlation coefficient tell us which pairs of parameters are related. Because this analysis is not designed to test any hypothesis in particular, it may be most useful in formulating new hypotheses. Two new hypotheses suggested by the data are as follows.

Since nacre angle spread and maximum temperature are highly correlated, it is possible that *the co-orientation of nacre tablets in bivalves is directly affected by water temperature* (hypothesis 1). This hypothesis is supported in at least one shell, the only shell studied by SIMS in sufficient detail, as shown in Figure 6. In addition, the data of Figure 6 suggest that tablet angle spread responds immediately to water temperature. The evolutionary or structural advantages of co-orientation or misorientation of nacre tablets (or any other biomineral) are unclear at this time. The fact that the strong correlation is neither with mean annual temperature nor with minimum temperature may be extremely significant. It suggests that nacre is preferentially deposited, and that aragonite tablets grow faster, when the temperature is higher. This inference is supported by Lowenstam's observation that more aragonite than calcite is deposited in mollusk shells at higher temperature.[67] Abiotically, calcium carbonates grow faster at higher water temperatures.[71−73] It is possible that the thermodynamic driving force at high temperatures overwhelms mollusk crystal growth control mechanisms[74] and may be the origin of the greater angle spreads observed in biogenic aragonite in nacre.

Because nacre tablet thickness and maximum pressure are highly correlated, it is possible that *mollusks (especially nautiloids) adapted, during the course of their evolution or during the life of each mollusk, to higher maximum pressures by reducing the thickness of their nacre tablets* (hypothesis 2). The idea that nacre tablet thickness is inversely proportional to mechanical resilience may be substantiated by future mechanical tests.

Both hypotheses must be verified by decoupling the effects of temperature and pressure from each other, by studying shells from the same family that live at a variety of temperatures or a variety of pressures.

CONCLUSIONS

We showed that the ultrastructure of nacre is sensitive to the environmental pressure and temperature in which the mollusks live and to which they have adapted. This sensitivity suggests that it may be possible to determine the maximum temperatures at which a certain mollusk, extant or extinct, lived by measuring the angle spread in its nacre crystals, thus using nacre as a thermometer. Ironically, we revealed this possibility by using high-resolution imaging but then integrated all the microscopic information into the strongly averaged data of Figure 5. This means that access to XANES-PEEM is not required to measure average angle spreads; in fact, X-ray diffraction experiments can measure the footprint of a rocking curve[23,30,37,75] or of a pole figure.[36,62] Also electron backscattered diffraction[76] or direct imaging of partly etched tablets[77] could give the same information, using scanning electron microscopy. Naturally, before nacre crystal misorientation can be used reliably as a thermometer or paleothermometer of ancient climates, extensive validation is necessary and cross-validation with well-established stable isotope geochemistry methods. Once validated, nacre paleothermometry has immediate and far-reaching implications: it would provide the maximum temperature at which a fossil ammonite lived and formed its shell, but also, using the tablet thickness−pressure correlation, it provides an estimate of the maximum depth at which the mollusk lived. This combination of temperature and distance from the water surface may prove valuable to reconstruct ancient climate on a time scale potentially spanning 450 million years.

METHODS SUMMARY

The shells of the eight mollusk species were cut, embedded, and polished perpendicularly to the nacre layers. They were then coated with Pt and analyzed with PEEM-3 on beamline 11.0.1 at the Berkeley-Advanced Light Source. Nineteen images were collected at the same 290.3 eV photon energy, and a sample voltage of −15 kV, while the linear polarization vector was rotated between 0° and 90° in 5° increments. Each pixel of these stacks of 19 images, therefore, contained the polarization-dependence curve, which was fit to the function $A + B\cos^2(\mathrm{EPU}^\circ + \theta')$, in which the fit parameter θ' was optimized, measured, and displayed as a quantitative gray level as shown in Figure 3. The analysis was repeated for all 10^6 pixels in each stack of 20 μm × 20 μm images, with 20-nm pixel size. Angle spread measurements were taken as the "footprint" of the distribution of all θ' angles observed in individual PIC-maps, as shown in Supporting Information Figures S1−S4. *In situ* oxygen isotope data were acquired in the WiscSIMS Laboratory at UW-Madison by a CAMECA ims-1280 large radius multicollector ion microprobe. Full SIMS data are provided in the Supporting Information in a spreadsheet file. Detailed methods are also described in Supporting Information.

ASSOCIATED CONTENT

Supporting Information

Detailed methods, additional figures, and spreadsheet with full SIMS data. This material is available free of charge via the Internet at http://pubs.acs.org.

AUTHOR INFORMATION

Corresponding Author

pupa@physics.wisc.edu

Notes

The authors declare no competing financial interest.
P.U.P.A. Gilbert previously published as Gelsomina De Stasio.

ACKNOWLEDGMENTS

We thank Sabine Gross for providing the *Lasmigona complanata* shells, and Lisie Kitchel for identifying their species, Antonio Checa for providing the *Bathymodiolus azoricus* shells, Darrel Ramsey-Musolf, Michael Ramsey-Musolf, Susan N. Coppersmith, and Laurence Loewe for discussions, and Steve Weiner for reading an early version of this manuscript. We acknowledge the expert technical support of beamline scientists Andreas Scholl, Anthony Young, and Andrew Doran during the PEEM-3 experiments, and that of Yutao Gong for data acquisition. We thank Brian Hess and John Fournelle for SIMS sample preparations and imaging. This work was supported by NSF awards CHE-0613972 and DMR-1105167, DOE Award DE-FG02-07ER15899, and UW-Hamel Award to PUPAG. The PEEM experiments were performed at the Berkeley Advanced Light Source, supported by DOE under contract DE-AC02-05CH11231. WiscSIMS is partially supported by NSF-EAR awards 0319230, 0744079, and 1053466.

REFERENCES

(1) Addadi, L.; Weiner, S. *Nature* **1997**, *389*, 912.
(2) Hare, P. E.; Abelson, P. H. *Year Book − Carnegie Inst. Washington* **1965**, *64*, 223.
(3) Mutvei, H. *Lethaia* **1983**, *16*, 233.
(4) Mutvei, H.; Dunca, E. *Palaeontol. Z.* **2010**, *84*, 457.
(5) Vendrasco, M. J.; Checa, A. G.; Kouchinsky, A. V. *Palaeontology* **2011**, *54*, 825.
(6) Currey, J. D. *Proc. R. Soc. London, Ser. B* **1977**, *196*, 443.
(7) Gao, H. J.; Ji, B. H.; Jager, I. L.; Arzt, E.; Fratzl, P. *Proc. Natl. Acad. Sci. U.S.A.* **2003**, *100*, 5597.
(8) Smith, B. L.; Schäffer, T. E.; Viani, M.; Thompson, J. B.; Frederick, N. A.; Kindt, J.; Belcher, A.; Stucky, G. D.; Morse, D. E.; Hansma, P. K. *Nature* **1999**, *399*, 761.
(9) Sellinger, A.; Weiss, P. M.; Nguyen, A.; Lu, Y. F.; Assink, R. A.; Gong, W. L.; Brinker, C. J. *Nature* **1998**, *394*, 256.
(10) Tang, Z. Y.; Kotov, N. A.; Magonov, S.; Ozturk, B. *Nat. Mater.* **2003**, *2*, 413.
(11) Fritz, M.; Belcher, A. M.; Radmacher, M.; Walters, D. A.; Hansma, P. K.; Stucky, G. D.; Morse, D. E.; Mann, S. *Nature* **1994**, *371*, 49.
(12) Rousseau, M.; Lopez, E.; Stempflé, P.; Brendlé, M.; Franke, L.; Guette, A.; Naslain, R.; Bourrat, X. *Biomaterials* **2005**, *26*, 6254.
(13) Cartwright, J. H. E.; Checa, A. G.; Escribano, B.; Sainz-Diaz, C. I. *Proc. Natl. Acad. Sci. U.S.A.* **2009**, *106*, 10499.
(14) Metzler, R. A.; Abrecht, M.; Olabisi, R. M.; Ariosa, D.; Johnson, C. J.; Frazer, B. H.; Coppersmith, S. N.; Gilbert, P. *Phys. Rev. Lett.* **2007**, *98*, 268102.
(15) Checa, A. G.; Cartwright, J. H. E.; Willinger, M. G. *Proc. Natl. Acad. Sci. U.S.A.* **2009**, *106*, 38.
(16) Nudelman, F.; Gotliv, B. A.; Addadi, L.; Weiner, S. *J. Struct. Biol.* **2006**, *153*, 176.
(17) Schäffer, T. E.; Ionescu-Zanetti, C.; Proksch, R.; Fritz, M.; Walters, D. A.; Almqvist, N.; Zaremba, C. M.; Belcher, A. M.; Smith, B. L.; Stucky, G. D.; Morse, D. E.; Hansma, P. K. *Chem. Mater.* **1997**, *9*, 1731.
(18) Gilbert, P. U. P. A; Metzler, R.; Zhou, D.; Scholl, A.; Doran, A.; Young, A.; Kunz, M.; Tamura, N.; Coppersmith, S. *J. Am. Chem. Soc.* **2008**, *130*, 17519.
(19) Wise, S. W. *Science* **1970**, *167*, 1486.

(20) Rousseau, M.; Lopez, E.; Coute, A.; Mascarel, G.; Smith, D. C.; Naslain, R.; Bourrat, X. *J. Struct. Biol.* **2005**, *149*, 149.
(21) Stohr, J.; Baberschke, K.; Jaeger, R.; Treichler, R.; Brennan, S. *Phys. Rev. Lett.* **1981**, *47*, 381.
(22) Ade, H.; Hsiao, B. *Science* **1993**, *262*, 1427.
(23) Metzler, R. A.; Zhou, D.; Abrecht, M.; Chiou, J. W.; Guo, J. H.; Ariosa, D.; Coppersmith, S. N.; Gilbert, P. U. P. A. *Phys. Rev. B* **2008**, *77*, 064110.
(24) Gilbert, P. U. P. A; Young, A.; Coppersmith, S. N. *Proc. Natl. Acad. Sci. U.S.A.* **2011**, *108*, 11350.
(25) Frazer, B. H.; Gilbert, B.; Sonderegger, B. R.; De Stasio, G. *Surf. Sci.* **2003**, *537*, 161.
(26) Gilbert, P. U. P. A.; Frazer, B. H.; Abrecht, M. In *Molecular Geomicrobiology*; Banfield, J. F., Nealson, K. H., Cervini-Silva, J., Eds.; Mineralogical Society of America: Washington, DC, 2005; Vol. *59*, p 1570185.
(27) Wise, S. W. *Eclogae Geol. Helv.* **1970**, *63*, 775.
(28) Taylor, J. D. *Paleontology* **1973**, *16*, 519.
(29) Hedegaard, C.; Wenk, H. R. *J. Mollusc. Stud.* **1998**, *64*, 133.
(30) Chateigner, D.; Hedegaard, C.; Wenk, H. R. *J. Struct. Geol.* **2000**, *22*, 1723.
(31) Lowenstam, H. A. *Science* **1981**, *211*, 1126.
(32) Mann, S. *Biomineralization: Principles and Concepts in Bioinorganic Materials Chemistry*; Oxford University Press: New York, 2001.
(33) Zhang, X. A.; Wu, W. J.; Wang, J. F. *Chin. Sci. Bull.* **2007**, *52*, 3452.
(34) Lee, S. W. *Mater. Charact.* **2009**, *60*, 980.
(35) Freer, A.; Greenwood, D.; Chung, P.; Pannell, C. L.; Cusack, M. *Cryst. Growth Des.* **2009**, *10*, 344.
(36) Checa, A. G.; Rodríguez-Navarro, A. B. *Biomaterials* **2005**, *26*, 1071.
(37) Cartwright, J. H. E.; Checa, A. G. *J. R. Soc. Interface* **2007**, *4*, 491.
(38) DiMasi, E.; Sarikaya, M. *J. Mater. Res.* **2004**, *19*, 1471.
(39) Erben, H. K. *Biomineralisation* **1972**, *4*, 15.
(40) Mutvei, H. *Zool. Scr.* **1978**, *7*, 287.
(41) Mutvei, H.; Dunca, E. *Palaeontol. Z.* **2008**, *82*, 85.
(42) Dauphin, Y.; Cuif, J.; Mutvei, H.; Denis, A. *Bull. Geol. Inst. Univ. Uppsala* **1989**, *15*, 7.
(43) Abbott, R. *American Seashells; The Marine Molluska of the Atlantic and Pacific Coasts of North America*; Van Nostrand Reinhold: New York, 1974.
(44) NOAA National Data Buoy Center, Station NPSF1, 8725110, Naples, FL, 2011.
(45) Kadar, E.; Checa, A. G.; Oliveira, A. N. D. P.; Machado, J. P. *J. Comp. Physiol., B* **2008**, *178*, 123.
(46) Gray, B. E.; Smith, A. M. *Pac. Sci.* **2004**, *58*, 47.
(47) NOAA NODC World Ocean Database. All available casts from 172.5E to 177E, 38.5S to 39.5S, 2011.
(48) Shepherd, S.; Turner, J. *J. Exp. Mar. Biol. Ecol.* **1985**, *93*, 285.
(49) NOAA National Data Buoy Center, Station MTYC1, 9413450, Monterey, CA, 2011.
(50) Baker, F. C. *Wisc. Geol. Nat. Hist. Surv. Bull.* **1928**, *70*, 1.
(51) USGS National Water Information System, Site 04087000, 2011.
(52) Seed, R.; Suchanek, T. H.; Gosling, E., 1992.
(53) NOAA National Data Buoy Center, Station PRYC1, 9415020, Point Reyes, CA, 2011.
(54) Saunders, W. B.; Ward, P. D. In *Nautilus, the biology and paleobiology of a living fossil*; Saunders, W. B., Landman, N. H., Eds.; Springer: Dordrecht, 2009 re-print, p 137.
(55) NOAA NODC World Ocean Database. Casts at 121.47E 5.58N, 120.63E 6.03N, 120.40E 6.43N, 120.10E 6.73N, 2011.
(56) NOAA Pacific Marine Environmental Laboratory Tropical Atmosphere Ocean Project. Data buoys at 137E 5N, 100E 8S, 2011.
(57) Gervis, M. H.; Sims, N. A. *The biology and culture of pearl oysters (Bivalvia: Pteriidae)*; ICLARM: Manila, Philippines, 1992; Vol. *21*.
(58) NOAA Pacific Marine Environmental Laboratory Tropical Atmosphere Ocean Project. Data buoy at 155W 8S, 2011.
(59) Mutvei, H. In *Biomineralization and Biological Metal Accumulation*; Westbroek, P., De Jong, E. W., Eds.; D. Reidel Publishing Co.: Dordrecht, Holland, 1982; p 267.
(60) Mayer, G. *Science* **2005**, *310*, 1144.
(61) Wang, R.; Suo, Z.; Evans, A.; Yao, N.; Aksay, I. *J. Mater. Res.* **2001**, *16*, 2485.
(62) Zaremba, C. M.; Belcher, A. M.; Fritz, M.; Li, Y. L.; Mann, S.; Hansma, P. K.; Morse, D. E.; Speck, J. S.; Stucky, G. D. *Chem. Mater.* **1996**, *8*, 679.
(63) Urey, H. C. *J. Chem. Soc.* **1947**, *1*, 562.
(64) Grossman, E. L.; Ku, T.-L. *Chem. Geol. (Isot. Geosci.)* **1986**, *59*, 59.
(65) Kim, S.-T.; O'Neil, J. R. *Geochim. Cosmochim. Acta* **1997**, *61*, 3461.
(66) Lowenstam, H. A. *J. Geol.* **1954**, *62*, 284.
(67) Lowenstam, H. A. *Proc. Natl. Acad. Sci. U.S.A.* **1954**, *40*, 39.
(68) Romanek, C.; Jones, D.; Williams, D.; Krantz, D.; Radtke, R. *Mar. Biol.* **1987**, *94*, 385.
(69) Wada, K. *Biomineralisation* **1972**, *6*, 141.
(70) Checa, A. G.; Jiménez-López, C.; Rodríguez-Navarro, A.; Machado, J. P. *Mar. Biol.* **2007**, *150*, 819.
(71) Morse, J. W.; Zullig, J. J.; Bernstein, L. D.; Millero, F. J.; Milne, P.; Mucci, A.; Choppin, G. R. *Am. J. Sci.* **1985**, *285*, 147.
(72) Zuddas, P.; Mucci, A. *Geochim. Cosmochim. Acta* **1994**, *58*, 4353.
(73) Zuddas, P.; Mucci, A. *Geochim. Cosmochim. Acta* **1998**, *62*, 757.
(74) Teng, H. H.; Dove, P. M.; Orme, C. A.; De Yoreo, J. J. *Science* **1998**, *282*, 724.
(75) Chateigner, D.; Ouhenia, S.; Krauss, C.; Hedegaard, C.; Gil, O.; Morales, M.; Lutterotti, L.; Rousseau, M.; Lopez, E. *Mater. Sci. Eng., A* **2010**, *528*, 37.
(76) Pérez-Huerta, A.; Dauphin, Y.; Cuif, J. P.; Cusack, M. *Micron* **2011**, *42*, 246.
(77) Mutvei, H. *Biomineralisation* **1972**, *4*, 81.